ACOUSTICS 2012

Experimental investigation of the aerodynamic noise radiated by a three-dimensional bluff body

J. Fischer, L.-E. Brizzi, J. Laumonier and V. Valeau

Institut Pprime, CNRS - Université de Poitiers - ENSMA, ENSIP, 6 rue Marcel Doré, Batiment B17, BP 633, 86022 Poitiers, France
jeoffrey.fischer@univ-poitiers.fr

Aerodynamic noise reduction is an important aspect for the development of cars in the automotive industry. The present work is an experimental study of the aerodynamic noise radiated by a three-dimensional simplified automotive model. The flow around this body is investigated using velocity (PIV), wall-pressure and far-field acoustic measurements in an anechoic wind-tunnel at low Mach number (below 0.15). After an aerodynamic characterisation of the generated flow focusing in particular on the A-pillar vortex, the goal is to study the localization of acoustic sources in the vicinity of the model. Therefore, some array processing techniques based on the beamforming technique are performed by using an Underbrink multi-arm spiral array located laterally and above the model. Results show the contribution of different noise sources (forward-facing ramp, roof, A-pillar vortex and strut) depending on frequency and demonstrate that the interaction of the A-pillar vortex with the body is the main source of aerodynamic sound over a large frequency range.

1 Introduction

The aeroacoustic noise generated by automotive in motion has been a relevant subject for the last decades as car manufacturers are interested in reducing it. That noise is caused by the development of aerodynamic structures from different parts of the vehicle (side mirrors, side windows, etc. [1]) and their interaction with the vehicle body. The present work focuses on one of these structures, the A-pillar vortex, which develops along the front side windows. The A-pillar vortex belongs to the family of unsteady separated flows which are characterized by a large-scale dynamic having a strong impact on the wall-pressure fluctuations. This three-dimensional structure is the result of (i) a detachment of the air flow due to lateral sharp edges, (ii) the winding of a vortex sheet and (iii) the reattachment of this conical vortex on the lateral sides of the body [2].

Experiments have been carried out with a bluff body representing a simplified car model called the MOPET (MOdèle Pour l'Étude des Tourbillons) which is presented in Figure 1. Some works on the aerodynamic characterisation of the vortex structure generated on the sides of this model have already been published [2, 3, 4]. These works have shown the existence of a secondary vortex inside and contra-rotated to the primary one. Although the general features of the flow dynamics of the A-pillar vortex are now well established, less is known concerning the acoustic radiation generated by the interaction of such a structure with the body. Our objective is thus to supplement these aerodynamic investigations with acoustic measurements.

First, the experimental set-up and instrumentation are detailed. Then, an aerodynamic characterisation of the A-pillar structure through velocity and wall-pressure measurements is used to validate the present experimental apparatus in comparison with available results. The last part consists of an acoustic investigation of the noise generated by the body. For this purpose, the beamforming technique has been used here to assess the main sources of sound generated by the interaction of the body with the flow.

2 Experimental set-up

Measurements were performed in the 3/4 open throat anechoic wind tunnel EOLE of the PPRIME Institute in Poitiers. The nozzle exit has a square cross-section of 460mm x 460mm and the test section has a length of 1.32m. A plywood plate connects the exit of the nozzle to the collector bounding the flow on its lower part. The acquisition system used for all the measurements is a 32 synchronised channels *ETEP* system. Measurements were carried out at U_∞ = 30, 40 and 50 m/s which is the maximum operating wind speed allowed by the system and corresponds to a Mach number of 0.15. The Reynolds number Re_H based on the height of the model is then in the range [$1.8.10^5$ - 3.10^5].

The body's length, width and height are respectively L=400 mm, W=120 mm and H=90 mm (Figure 1). The angle of the forward facing ramp is 30° while the two lateral sides are inclined at 10°. All angles are sharp except the junction between the ramp and the roof which is rounded in order to prevent flow separation. The distance between the exit section of the wind tunnel and the nose of the body is 220 mm and the height of the model from the bottom plate is 100 mm. These locations are based on the work of Hoarau [3]. The strut is shifted 250mm downstream via a metallic bar. Our motivation here was to separate the acoustic sources generated by the body from those generated by the strut. The blockage ratio of the body with its strut is 6%.

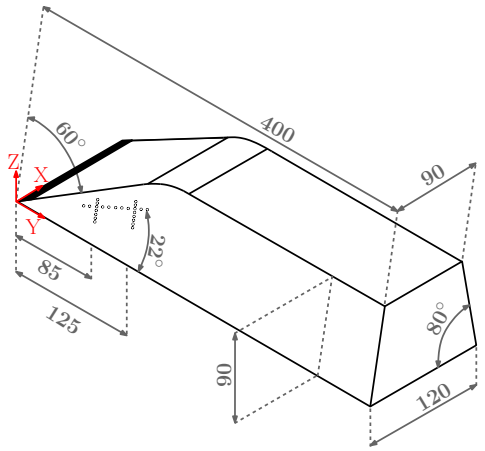

Figure 1: Dimensions of the body (in mm).

Wall-pressure measurements were performed on the lateral sides of the body using pressure probes *SensorTechnics*. The probes are disposed along 3 lines as shown in Figure 2. The angle between line L_T and the bottom of the model is 22° and the sensors are equally spaced at 7.25 mm. Lines L_1 and L_2 are vertical and have a common sensor with L_T. Sensors are spaced of 4 mm on L_1 and 6 mm on L_2. Due to material strains, only 16 probes can be used simultaneously. The probes are connected to pressure tabs via flexible tubes of 1 m length. The mean pressure of each probe (without fluctuation) is obtained with a buffer volume that attenuates the fluctuations. Finally, the recorded signal is the fluctuating pressure obtained by subtracting the instantaneous pressure with the mean pressure. The sensors are differential with a bandwidth of [0 Hz-1.6kHz] and a pressure range of 1250 Pa. The sampling frequency of the wall-pressure measure-

ments is 6250 Hz. Each probe's frequency response is measured using a coupler and a reference microphone *Brüel & Kjaer*. Thus, the corrected signals can be obtained by using the calculated transfer function. In the frequency domain, the frequency functions (auto and cross-spectra) are corrected in magnitude and phase with the transfer function. In the time domain, the measured signals are convolved with the impulse response, obtained by inverse Fourier transform of the transfer function.

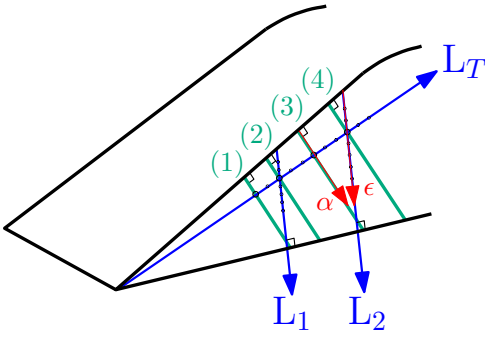

Figure 2: Wall-pressure probe lines are in blue, locations of the 4 PIV planes orthogonal to the forward facing ramp are in green and definitions of the axes α and ϵ are in red.

The velocity fields are obtained with Particle Image Velocimetry (PIV). The material used for the PIV measurements is a Nd-Yag LASER *QUANTEL* and a *LAVISION* Intense camera with a resolution of 1376 x 1040 pixels. Two components of the velocity are estimated in 4 planes orthogonal to the forward facing ramp and each plane is aligned with a sensor of L_T (Fig. 2). Statistics were performed over 2500 fields with a sampling frequency of 2 Hz. The size of the fields is 102mm x 77mm.

Acoustic microphones were used to estimate the far-field acoustic pressure signature of the aerodynamic noise generated by the body. Measurements were performed with a planar acoustic array consisting of 30 1/4-inch *B&K* microphones, model 4957. The bandwidth of the microphones is [50 Hz-10kHz] and the sampling frequency is 50 kHz. The calibration of each microphone is done with a calibrator delivering a sine wave at 1 kHz with an amplitude of 94 dB. The design of the array is an Underbrink multi-arm spiral [5] composed of 5 arms of 6 microphones. That design is very effective when searching for wide-band noise sources [6] which is the case here. The array is placed both laterally and above the model, outside the flow. A picture of the vertical array and the body is presented in Figure 3.

3 Aerodynamic characterisation

The flow structure has been described by Moraes [2] who has proposed a schematic description of the averaged A-pillar vortex. A view in the (X,Z) plane is proposed in Figure 4. The airflow first reaches the facing ramp of the model before separating onto the two lateral sides. The sheet of air then detaches from the model at the first separation point and rolls up in the (X,Z) plane while progressing downstream. That structure then reattaches to the model at a reattachment point. Even though this structure is unsteady it is characterized by a statistically mean position. That unsteady three-dimensional structure composes the primary vortex. A secondary vortex

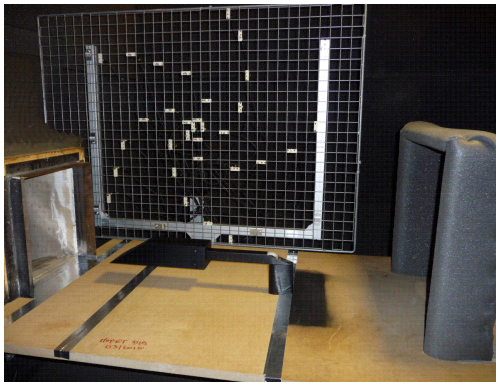

Figure 3: Picture of the MOPET body and the array. The flow goes from the left to the right.

also develops between the primary vortex and the model. Its separation point is a little over the mean centre of the primary vortex and it rotates in the opposite direction of the primary vortex.

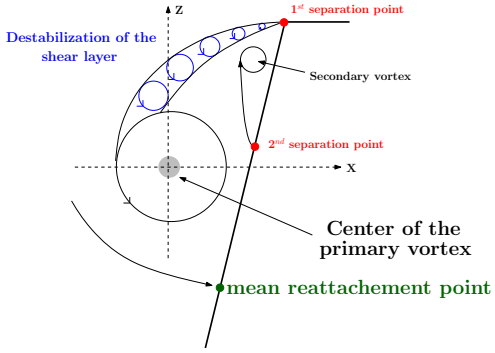

Figure 4: Schematic view of the phenomenon [2]

We define 2 axis : ϵ along L_2 and α along the 3^{rd} PIV plane. These axis start at the top lateral edge as shown in Figure 2. We also define α_0 the position of the mean reattachment point along α and ϵ_0 the same position along ϵ. Aerodynamic results will be shown using dimensionless axis ϵ/ϵ_0 and α/α_0.

Each velocity field measurements have been carried out at three different wind speeds (30, 40 and 50 m/s). The velocity field in PIV plane n°3 at U_∞ = 40 m/s is showed in Figure 5 (point A indicates the centre of the primary vortex). The influence of the Reynolds number on the position of the vortex (mean centre and mean reattachment point) has been studied. Results are not shown here for brevity. The conclusions of this study is that Re_H has little influence on the locations of the mean centre and mean reattachment of the vortex (maximum 1 mm). Moreover, the angles of the mean centre and the mean reattachment line of the vortex with the lower part of the MOPET have been calculated. They are 22.2° for the mean centre and 17.4° for the mean reattachment.

Measurements of velocity fields have also been carried out in 4 PIV planes (Figure 2). This study has shown that the mean reattachment line of the primary vortex passes through the leading edge of the model.

The fluctuating pressure coefficient Cp' of the wall-pressure is defined as

$$Cp' = \frac{\sqrt{< p'^2 >}}{1/2\rho U_\infty^2} \quad , \tag{1}$$

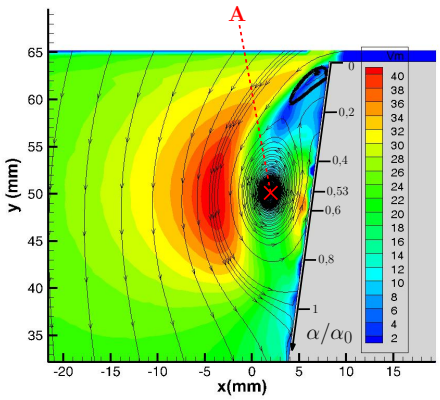

Figure 5: Mean velocity field in the plane n°3 at U_∞ = 40 m/s. Point A indicates the centre of the primary vortex.

where $< p'^2 >$ stands for the variance of the fluctuating wall-pressure signal and ρ the fluid density (air). The pressure signal p' has previously been low-pass filtered at 1.6 kHz which is the probes cut-off frequency. The Cp' coefficient has been estimated along line L_2 at 3 different wind speeds (Figure 6). Two maxima are present at ϵ/ϵ_0 = 0.47 and ϵ/ϵ_0 = 0.82. These results are similar to Moraes [2] who explained that these peaks correspond to spatial areas where the flow is very unsteady. The locations of these maxima can be transposed on the PIV visualisation. Knowing that the mean reattachment line passes through the nose, α_0 and ϵ_0, the positions ϵ/ϵ_0 = 0.47 and ϵ/ϵ_0 = 0.82 correspond respectively to α/α_0 = 0.38 and α/α_0 = 0.79. The first maximum of Cp' (α/α_0 = 0.38) is located in the detachment area of the secondary vortex (Figure 5) while the second maximum is a little over the mean reattachment of the primary vortex. That means that these two locations are very unsteady and sensitive to a spatial variation of the structure.

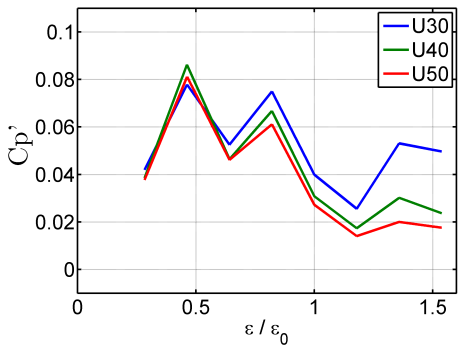

Figure 6: Cp' coefficient along line L_2 at U_∞ = 30 m/s (blue), 40 m/s (green) and 50 m/s (red).

4 Acoustic study via beamforming

4.1 Presentation of the array processing methods

Although the acoustic results are investigated with the conventional beamforming, other complementary techniques have been used and are presented below.

4.1.1 Beamforming presentation

The beamforming technique is a method for the localization of sound sources. The principle is to assume that, in a certain plane where the acoustic source is supposed to be, any point can be a source of sound. Let $s_m(t)$ denote the signal measured by the m^{th} microphone ($1 \leq m \leq M$). The plane in which the source is sought is divided into N grid points. For each point n ($1 \leq n \leq N$) located at a position $\mathbf{r_n}$ considered in this plane, the signals of all the microphones are delayed by a time shift $\Delta t_{m,n}$ which is the theoretical acoustic propagation time from the n^{th} point of the plane to the m^{th} microphone, and summed over all the microphones. The delay-and-sum beamformer's output signal can be expressed as [6, 7] :

$$z(\mathbf{r_n}, t) = \sum_{m=1}^{M} w_m s_m(t - \Delta t_{m,n}) \qquad (2)$$

The amplitude weight w_m accounting for geometrical attenuation are set to 1 in this paper. When the sound sources are stationary, the beamforming method is more efficient when computed in the frequency domain. Its expression is then [6, 7] :

$$\mathbf{Z}(\mathbf{r_n}, f) = \frac{\mathbf{e}^T \mathbf{W} \mathbf{G} \mathbf{W}^T \mathbf{e}}{(\sum_{m=1}^{M} w_m)^2} \quad , \qquad (3)$$

where $\mathbf{G}$ is the [MxM] cross spectral density matrix of the measured signals, $\mathbf{e}$ the [1xM] frequency-dependent steering vector $e^{-j2\pi f \Delta t_{m,n}}$, $\mathbf{W}$ the [MxM] diagonal matrix containing the values of w_m and ^{T} denotes the conjugate transposed operator. Note that the resulting function $\mathbf{Z}$ depends on the frequency f which means that the beamforming output is considered at a given frequency.

One of the drawbacks of that method is the dependency of the resolution with frequency. The resolution is defined as the size of the lobe at -3dB. Figure 7 shows the result of the beamforming algorithm for a numerical wide-band noise source located at the centre of the map at two frequencies f = 500Hz and f = 3kHz. The resolution is then 73 cm for f = 500Hz and 8 cm for f = 3kHz. Note that calculations are not done at one specific frequency but in a frequency band of 100 Hz centred in f. In this paper, the acoustic levels shown on beamforming maps are those of the Power Spectral Density (PSD) expressed in dB (reference = 2.10^5 Pa). As observed in Figure 7, the resolution improves when frequency increases. That is a major observation to retain for the following results.

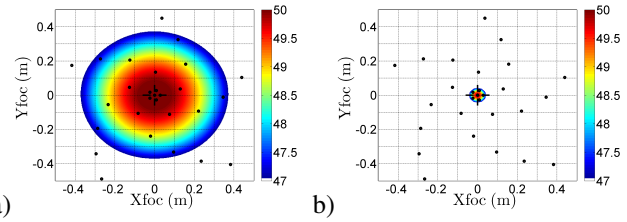

a) b)

Figure 7: Beamforming result for a numerical wide-band noise source located at (X = 0 m, Y = 0 m, Z = 1 m) at f = 500 Hz (left) and f = 3 kHz (right). Black circles correspond to microphone positions. Level of PSD is in dB.

4.1.2 Background noise deletion

The anechoic wind-tunnel has been carefully designed to minimise the overall background noise. However, the weakness of the levels generated by aerodynamic noise can prevent a satisfying imaging of the aerodynamic sound sources and specific denoising techniques have to be applied. Figure 8a shows that the sound differential between the aeroacoustic noise of the body and the background noise is very weak (maximum 3dB).

A particularly efficient technique generally used in beamforming is the background noise deletion [8]. It consists in measuring the background noise of the wind tunnel (without the model) and removing its cross spectral matrix from the one obtained with the model in the flow. The expression of the array output in equation (3) becomes :

$$\mathbf{Z}(\mathbf{r_n}, f) = \frac{\mathbf{e}^T \mathbf{W}(\mathbf{G} - \mathbf{G_{back}})\mathbf{W}^T \mathbf{e}}{(\sum_{m=1}^{M} w_m)^2} \quad , \tag{4}$$

where $\mathbf{G_{back}}$ refers to the cross spectral density matrix of the background noise (without the model in the flow). Figure 8 shows the effect of that technique for a measurement on the model at U_∞ = 40 m/s and at f = 2500 Hz. The efficiency of background noise deletion is clearly visible as the model parts responsible for sound emission clearly appear after noise deletion.

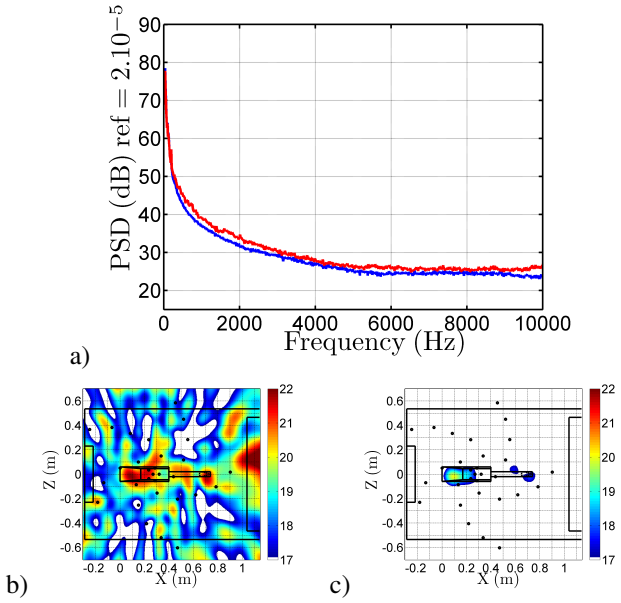

Figure 8: a) PSD of the signal of a microphone of the array without (blue) and with (red) the body present. Beamforming result without (b) and with (c) background noise deletion. U_∞ = 40 m/s, f = 2500 Hz. Black circles correspond to microphone positions. Level of PSD is in dB.

4.1.3 Flow effects on propagation

During their propagation from the source to the array, the wavefronts undergo some substantial convection and refraction effects. If they are not taken into account, this can lead to an apparent shift of the sound source region in the downstream direction. At low Mach number (< 0.3) this apparent shift can be satisfactorily estimated by the product of the Mach number and the mean flow thickness [9]. In this study, this apparent shift ranges around 2 cm and the beamforming results were corrected to compensate this shift.

4.2 Beamforming results

Beamforming results of the MOPET in flow at U_∞ = 40 m/s with the two arrays (horizontal and vertical) are presented in Figure 9 for 3 frequencies. Note that horizontal and vertical measurements have been done separately.

The beamforming calculation has been carried out for many frequencies and the phenomena observed in Figure 9 exist over larger frequency bands : [1.1 ; 1.7] kHz for 9a and 9d, [1.8 ; 3.9] kHz for 9b and 9e et [4 ; 6.5] kHz for 9c and 9f. Over 6.5 kHz, the array output becomes very noisy.

The first observation from Figure 9 is that the estimated locations of the acoustic sources are coherent seen from above and next to the model. However, a source coming from the strut is visible with the vertical array and not with the horizontal one. This apparent discrepancy could be explained by a sound source thats is strongly dipolar in nature, the axis of the dipole being horizontal and perpendicular to the flow. Watching from above, out-of-phase contributions of the dipole vanish by destructive interferences but watching laterally, only one contribution is visible and is then measured by the array.

Considering the acoustic sources coming only from the body, three source locations have been observed :

- the roof for $f \in$ [1.1 ; 1.7] kHz
- the forward-facing ramp for $f \in$ [1.8 ; 3.9] kHz
- the lateral sides for $f \in$ [4 ; 6.5] kHz.

As frequency increases, the sound source seems to move up to the front of the model. Moreover, the source at the forward-facing ramp (Figure 9b) separates into two lateral sources on each side of the model when frequency increases (Figure 9c). These sources are located at the A-pillar vortex positions, which means that the interaction of the A-pillar structure with the body is the actual emerging source on the model in a large frequency range, [4 ; 6.5] kHz. Actually, the sources might be separated at earlier frequencies but the frequency-dependent resolution is then too low to distinguish them. Indeed, the resolution at f = 3kHz is 8 cm which is about the width of the model, and at f = 4 kHz, the resolution is 6 cm. Therefore, the two lateral sources due to the A-pillar vortices might exist at lower frequencies (below 4 kHz) but the frequency-dependent resolution of the array output is masking that effect. A deconvolution method (DAMAS [10]) has been used to improve the resolution but the results were not satisfying.

5 Conclusion

The aerodynamic results have been confirmed by litterature [3]. Wall unsteady regions with a maximum fluctuating pressure coefficient have been located over the mean reattachment of the primary vortex and also on the detachment of the secondary vortex. Moreover, this work has shown the independence of the vortex mean position with the Reynolds number.

Acoustic measurements have shown that the sound differential between the aeroacoustic noise of the MOPET body

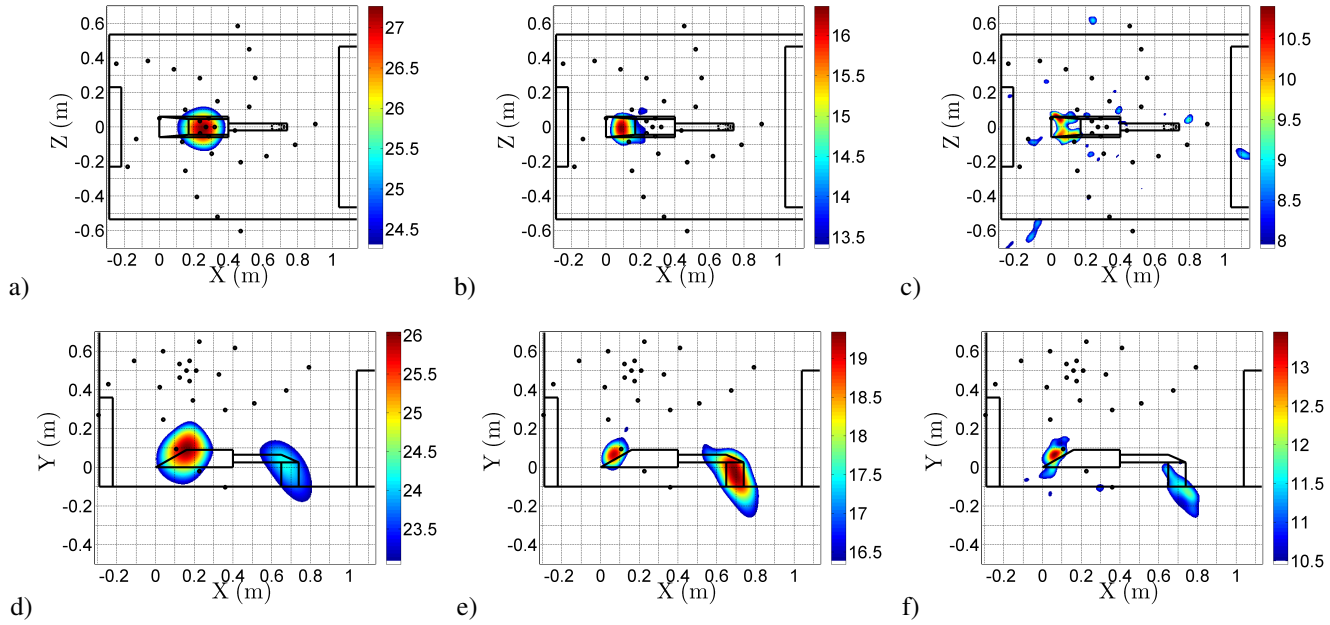

Figure 9: Beamforming result with horizontal (up) and vertical (down) array. f = 1.5 kHz for a) and d), f = 3kHz for b) and e), f = 5.5 kHz for c) and f). U_∞ = 40 m/s. Black circles correspond to microphone positions. Level of PSD is in dB.

and the wind-tunnel noise is very weak (maximum 3 dB) in a wide frequency range. Different sound source locations have been identified : the roof at low frequencies, the forward-facing ramp at middle frequencies and the lateral sides (A-pillar vortex locations) at higher frequencies (4 to 6.5 kHz). Moreover, the strut has also a wide-band acoustic signature but can be easily distinguished from the body noise.

It is likely that the lateral sound sources generated by the interaction of the A-pillar vortices with the body are distinguished only over 4 kHz because of an insufficient resolution of the beamforming technique at lower frequencies. The sound source apparently generated by the forward ramp could be the result of two sources emanating from the lateral edges, but indistinguishable from each other for this reason. It is indeed unlikely that the flat part of the forward facing ramp generates some significant noise as in this region the flow is attached and the wall-pressure fluctuations are weak compared to the lateral side ones. The two lateral acoustic sources due to A-pillar vortices activity should then exist at frequencies lower than 3 kHz. The lateral A-pillar structures are then the most important noise sources, in terms of frequency range, developing on the model. The A-pillar vortex is then both a region of strong aerodynamic fluctuations and of a wide-band acoustic emission. A study that is more dedicated to the link between wall-pressure and far-field acoustics is presently being carried out.

References

[1] W.H. Hucho *Aerodynamics of road vehicles: from fluid mechanics to vehicle engineering*, SAE, ISBN (1998)

[2] L.F. Gouveia de Moraes, *Analyse expérimentale d'un modèle de tourbillon conique et de sa sensibilité à une turbulence amont*, PhD., Université de Poitiers (2011)

[3] C. Hoarau, J. Borée, J. Laumonier, Y. Gervais, *Unsteady wall-pressure field of a model A-pillar conical vortex*, International Journal of Heat and Fluid Flow (2008)

[4] B. Levy, P. Brancher, A. Giovannini, *Experimental characterization of the velocity and wall-pressure fields of an A-pillar vortex*, 14th AIAA/CEAS Aeroacoustics Conference, Vancouver (2008)

[5] J.R. Underbrink, *Circularly symmetric, zero redundancy, planar array having broad frequency range applications*, U.S. patent No. 6,205,224 (2001)

[6] T.J. Mueller, *Aeroacoustic measurements*, Springer (2002)

[7] L. Koop *Beamforming methods in microphone array measurements. Theory, practice and limitations*, VKI lecture notes (2007)

[8] F.V. Hutcheson, T.F. Brooks, *Measurement of trailing edge noise using directional array and coherent output power methods*, International Journal of Aeroacoustics (2002)

[9] T. Padois, *Localisation de source acoustique en soufflerie anéchoïque par deux techniques d'antennerie : formation de voies et retournement temporel numérique*, PhD., Université de Poitiers (2011)

[10] T.F. Brooks, W.M. Humphreys, *A deconvolution approach for the mapping of acoustic sources (DAMAS) determined from phased microphone arrays*, Journal of Sound and Vibration (2006)